JOURNAL OF THERMOPHYSICS AND HEAT TRANSFER
Vol. 14, No. 4, October–December 2000

Modeling of Glow Radiation in the Rarefied Flow About an Orbiting Spacecraft

S. F. Gimelshein* and D. A. Levin†
George Washington University, Washington, D.C. 20052
and
R. J. Collins‡
University of Minnesota, Minneapolis, Minnesota 55455

An approach for modeling visible glow radiation about a spacecraft in low Earth orbit has been examined. A new technique for simulation of surface chemical reactions based on the direct simulation Monte Carlo method is used. The study focuses on the sensitivity of glow radiation to the gas-phase reaction model and surface reaction cross sections in the altitude range from 140 to 200 km. Comparison of predictions for different gas reaction cross sections and surface parameters is given with the Atmospheric Explorer data. It is shown that although the radiance is increased by a factor of two when a quasi-classical model is used, the altitude dependence of the predicted radiation is the same as that obtained using the total collisional energy model. Furthermore, it is found that the influence of the freestream NO concentration on the total radiation is small for altitudes up to 200 km. The main contribution is the formation of NO in bow-shock gas-phase reactions.

Nomenclature

A	=	preexponential factor in the Arrhenius expression
B	=	temperature exponent in the Arrhenius expression
E_a	=	activation energy
F_{num}	=	ratio of molecules to simulated particles
f_i	=	number flux of the ith species
H_s	=	heat of absorption
I	=	radiation intensity
k	=	Boltzmann constant, chemical rate constant
k_b	=	desorption rate
M	=	chemical species
N_i	=	number of collisions of species i with species j
n	=	number density
n_T	=	total number of surface sites
P	=	probability
S	=	vacant surface site
S_o	=	sticking coefficient
T	=	temperature
v	=	relative velocity, gas velocity
W_k	=	weighting factor of the kth species
Z_{ij}	=	collision frequency of species i with j
Δt	=	time step
$\sigma_{f3,f4}$	=	cross sections for glow production
σ_T	=	total collision cross section
τ_l	=	radiation lifetime

Subscript

S	=	surface adsorbed species

Superscript

$*$	=	electronically excited state

Received 21 December 1999; revision received 10 May 2000; accepted for publication 12 May 2000.

*Senior Research Scientist, Department of Chemistry. Member AIAA.
†Research Professor, Department of Chemistry. Senior Member AIAA.
‡Professor Emeritus, Department of Electrical Engineering.

I. Introduction

SPACECRAFT radiation is primarily caused by the interaction of spacecraft surfaces with the rarefied atmosphere in low Earth orbit. Detailed information on the physical and chemical processes that occur at the surface and in the gas phase is critical for understanding glow formation mechanisms and the experimental data accumulated in recent years. Numerical methods that enable one to simulate spacecraft glow are of importance because they can provide for very detailed data on the spacecraft local atmosphere, which has many important operational applications such as spacecraft contamination and optical sensor interference. In terms of numerical modeling, a key issue for further improving reliability is the use of accurate and adequate models for gas-phase and gas/surface collision processes. Development and application of efficient numerical models and algorithms for simulating these collisions is, therefore, critical for obtaining credible data on radiation phenomena.

It is well known[1] that the important spacecraft glow processes occur at high flight altitudes (higher than 100 km) where the effects of rarefaction play a determining role. The traditional computational fluid dynamics approaches based on solution of the Navier–Stokes or viscous shock layer equations fail at such rarefied conditions. Methods of rarefied gas dynamics therefore have to be used for modeling these processes. The most powerful method of rarefied gas dynamics is the direct simulation Monte Carlo (DSMC) method.[2] A recent approach for modeling surface processes has been developed in Refs. 3 and 4 that is suitable for the DSMC method. The adsorption and formation of new species on the surface was simulated in Ref. 3 using the DSMC method, and the visible glow from excited NO_2 was calculated for hypersonic flow around the Atmospheric Explorer and compared with experimental data.[5] The earlier work of Karipides et al.[6,7] also examined spacecraft glow using the DSMC method. The numerical approach used in this work is different in that an overlay approach is not used. Moreover, a different set of issues is examined here. The present paper uses the results of Refs. 3 and 4 and extends them to provide a more detailed explanation of spacecraft glow.

The main objectives of this work are to present an improved DSMC approach for modeling surface processes, to apply it for modeling glow radiation in an energetic flow around the Atmospheric Explorer (AE), and to study in detail the influence of gas-phase chemical reactions on NO_2 glow radiation. The DSMC approach presented here improves the efficiency of the computational procedure so that sufficient accuracy can be obtained at all altitudes of interest. Moreover, the high accuracy permits us to evaluate the sensitivity

of predicted radiation to changes in freestream conditions, chemistry models, surface models, and fully coupled vs analytic radiation models. Many of these comparisons involve small but physically meaningful differences where high accuracy is a necessity.

In the following section the chemical processes responsible for NO_2 glow at high altitudes are reviewed. Then, the description of a new DSMC procedure is presented that uses a weighting scheme for modeling chemical reactions in gas and on the surface. The principal differences between the present approach and previously used techniques[3] are discussed. After a brief discussion on flow conditions and utilized parameters of the DSMC method, the results of the computational study are given. The sensitivity of the glow radiation to the chemical reaction model and the freestream NO concentration is clarified. Comparison with analytic predictions is followed by the results obtained for different surface parameters. Finally, comparison of the numerical data with flight measurements is presented.

II. NO_2 Radiation Mechanisms

A. Surface Processes

The detailed description of processes occurring at spacecraft surfaces at high altitudes is given in the work of Dogra et al.[3] Here we mention only the most important features relevant to modeling the visible glow. The process responsible for glow in the visible portion of the spectrum[8] is the radiation of NO_2^* molecules formed by the recombination of atmospheric, hyperthermal $O(^3P)$ atoms with surface-adsorbed NO (here NO_2^* denotes an excited electronic state of NO_2).

The spacecraft surface is assumed to be a metal oxide. Surface bombardment by O and NO results in those species being physisorbed or weakly chemisorbed to the surface, as long as there are available sites. The principal process for surface glow follows an Eley–Rideal mechanism (see Ref. 9) with NO_2^* formed by subsequent collisions of O with surface-physisorbed NO. The formation of NO_2^* through the interaction of gas-phase NO and adsorbed O particles has also been considered in simulation, but not found to be significant. The second possible mechanism of NO_2^* formation, based on a Langmuir–Hinshelwood scheme including reaction of both surface adsorbed NO and O, was not considered due to the relatively low heat of adsorption values that are reasonable for a surface glow model.[3]

Hence, the major surface processes responsible for the visible glow originated from NO_2^* are summarized as follows:

$$NO + S \leftrightarrow NO_S \tag{1}$$

$$O + S \leftrightarrow O_S \tag{2}$$

$$O + NO_S \rightarrow NO_2 + S + h\nu \tag{3}$$

$$NO + O_S \rightarrow NO_2 + S + h\nu \tag{4}$$

$$M + NO_S \rightarrow M + NO + S \tag{5}$$

$$M + O_S \rightarrow M + O + S \tag{6}$$

where S represents a surface site available for physisorption. Reactions (1) and (2) are adsorption/desorption reactions, reactions (3) and (4) are glow processes, and reactions (5) and (6) are scrubbing reactions. Equations (3–6) are assumed to proceed only in the forward direction. The scrubbing processes involve all gas species (denoted as M), that is, N_2, O_2, NO, N, O, and NO_2.

The desorption rate constants [backwards processes in Eqs. (1) and (2)] are assumed to be temperature dependent and defined as

$$k_b = 10^{13} \exp(-H_s/kT_w),\ s^{-1}$$

where T_w is the wall temperature. The forward rate is derived from the inherent properties of the gas species incident on the surface and the surface material by use of S_o. The values of the surface parameters from Ref. 4 were used in this work. Table 1 provides their summary.

Table 1 Summary of surface glow parameters

Parameter	Range of values
NO heat of absorption, kcal/mole	16 (set 1) 20 (set 2)
O heat of absorption, kcal/mole	3
Sticking coefficients for adsorption processes S_o	0.5
Wall temperature T_w, K	300
Glow cross sections for processes (3) and (4) $\sigma_{f3,f4}$, Å^2	0.1
Scrubbing cross sections for processes (5) and (6) Å^2	0 (set 1) 4 (set 2)
Total number of surface sites per m^2, n_T	0.24×10^{20}

B. Gas-Phase Processes

A seven-species mixture consisting of N, O, N_2, O_2, NO, NO_2^*, and NO_2 was used. At the high altitudes studied, the impact of chemical reactions on major species N_2, O_2, and O is negligibly small. The reaction path

$$N_2 + O \rightarrow NO + N$$

is the single, dominant chemical reaction responsible for the formation of NO, which in turn controls the production of NO_2^*. This reaction is highly endothermic, but in the center of mass system of collisions between freestream and reflected particles there is sufficient collisional energy at these orbital conditions. The interaction of the wall with the reacting gas, therefore, affects the chemical reaction rate. These effects do not change the conclusions of this work and are reported elsewhere.[10] The full set of air chemical reactions has been modeled for the sake of completeness, including fifteen dissociation reactions and four exchange reactions. The list of reactions is given in Table 2 together with constants for the corresponding Arrhenius equations, $k = AT^{-B} \exp\{-E_a/kT\}$. Here, k is the reaction rate. The heat of reaction given in column 3 of Table 2 is the energy transferred between the translational, rotational, and vibrational modes of reagents (or reaction products for negative reaction heat values) and the potential energy of electronic levels of reaction products (or reagents for negative reaction heats). The values for the constants A, B, and E_c taken from earlier work[3] were used here.

The glow processes (3) and (4) comprise two components. The first is related to the formation of NO_2^* on the surface, and the second is the spontaneous emission $NO_2^* \rightarrow NO_2 + h\nu$ in the gas phase. The key parameter of the second stage is the average life time of NO_2^*, τ_l, which was assumed to equal 0.0003 s.

III. Numerical Method

A. General Approach

The DSMC-based computational tool, SMILE,[11] has been used in computations. The majorant frequency scheme of Ivanov and Rogasinsky[12] is employed for modeling molecular collisions. SMILE was modified respectively to account for surface reactions. Instead of a three-step approach based on an overlay concept used for modeling trace species gas-phase and surface reactions in earlier work,[3] a more efficient one-step algorithm was developed. A weighting scheme has been used to simulate both the elastic collision processes between major and trace species and the chemical reactions in gas phase and on the surface. The major and trace gas species in the flows discussed in this work are N_2, O_2, and O and NO, N, and NO_2, respectively. The most important gas/surface processes involve NO_S, Eqs. (1), (3), and (5). Consistent with the gas phase, NO_S is modeled as a trace species. It is emphasized that the use of a weighting procedure is indispensable for obtaining credible results on NO_2^* radiative processes due to very small relative concentrations of species important for radiation. The procedures enables one to increase drastically sample size of the trace species.

B. Weighting Scheme for Modeling Elastic Collisions

The elastic collisions were simulated using the weighting scheme[2] adopted for the majorant collision scheme. The weighting scheme

Table 2 List of gas-phase reactions

Reaction number	Reaction path	Enthalpy of reaction, J	A, mol · s/m^3	B	E_a, J
1	$O_2 + N \rightarrow O + O + N$	8.197×10^{-19}	5.993×10^{-12}	1	8.197×10^{-19}
2	$O_2 + NO \rightarrow O + O + NO$	8.197×10^{-19}	5.993×10^{-12}	1	8.197×10^{-19}
3	$O_2 + N_2 \rightarrow O + O + N_2$	8.197×10^{-19}	1.198×10^{-11}	1	8.197×10^{-19}
4	$O_2 + O_2 \rightarrow O + O + O_2$	8.197×10^{-19}	5.393×10^{-11}	1	8.197×10^{-19}
5	$O_2 + O \rightarrow O + O + O$	8.197×10^{-19}	1.498×10^{-10}	1	8.197×10^{-19}
6	$N_2 + O \rightarrow N + N + O$	1.561×10^{-18}	3.187×10^{-13}	0.5	1.561×10^{-18}
7	$N_2 + O_2 \rightarrow N + N + O_2$	1.561×10^{-18}	3.187×10^{-13}	0.5	1.561×10^{-18}
8	$N_2 + NO \rightarrow N + N + NO$	1.561×10^{-18}	3.187×10^{-13}	0.5	1.561×10^{-18}
9	$N_2 + N_2 \rightarrow N + N + N_2$	1.561×10^{-18}	7.968×10^{-13}	0.5	1.561×10^{-18}
10	$N_2 + N \rightarrow N + N + N$	1.561×10^{-18}	6.900×10^{-8}	1.5	1.561×10^{-18}
11	$NO + N_2 \rightarrow N + O + N_2$	1.043×10^{-18}	6.590×10^{-10}	1.5	1.043×10^{-18}
12	$NO + O_2 \rightarrow N + O + O_2$	1.043×10^{-18}	6.590×10^{-10}	1.5	1.043×10^{-18}
13	$NO + NO \rightarrow N + O + NO$	1.043×10^{-18}	1.318×10^{-8}	1.5	1.043×10^{-18}
14	$NO + O \rightarrow N + O + O$	1.043×10^{-18}	1.318×10^{-8}	1.5	1.043×10^{-18}
15	$NO + N \rightarrow N + O + N$	1.043×10^{-18}	1.318×10^{-8}	1.5	1.043×10^{-18}
16	$NO + O \rightarrow O_2 + N$	2.719×10^{-19}	5.279×10^{-21}	−1	2.719×10^{-19}
17	$N_2 + O \rightarrow NO + N$	5.175×10^{-19}	1.120×10^{-16}	0	5.175×10^{-19}
18	$O_2 + N \rightarrow NO + O$	-2.719×10^{-19}	1.598×10^{-18}	−0.5	4.968×10^{-20}
19	$NO + N \rightarrow N_2 + O$	-5.175×10^{-19}	2.490×10^{-17}	0	0

will be explained by its connection to the usual gas kinetic formulation. Let us introduce the following nomenclature and relationships:

W_k = species weighting factors (or weights), where $0 < W_k \leq 1$ and k is the species index
n_k = number of simulated particles, per unit volume, with weighting
n'_k = number of atoms or molecules per unit volume
F_{num} = conversion between molecules and simulated particles
σ'_T = total collision cross section as defined by Bird[2]

For σ'_T, $\sigma_T = \sigma'_T F_{\text{num}}$, where the prime indicates the properties of real molecules. The number of real molecules can be related to the number of simulated particles with weights by

$$n'_k = W_k F_{\text{num}} n_k \tag{7}$$

Major species are assigned a weighting factor value of unity, whereas trace species have a typical value of $W_k = 0.005$ in this work. Hence, the trace species concentrations are increased by a factor of $1/W_k$.

According to kinetic theory, a molecule of species i experiences N'_i collisions with species j in a time period Δt of

$$N'_i = n'_j \overline{\sigma'_T(v)v} \Delta t \tag{8}$$

with a collision frequency Z'_{ij}

$$Z'_{ij} = n'_j \overline{\sigma'_T(v)v} \tag{9}$$

where v is the relative velocity of the molecules and the bar indicates the average taken over a group of molecules. When the simulations are performed, we choose similar expressions for the number of collisions between simulated particles that will provide an efficient procedure and reduce to the gas kinetic result of Eqs. (8) and (9). For collisions between simulated particles the collision frequency may be written as

$$Z_{ij} = n_j \overline{\sigma_T(v)v} W_j \tag{10}$$

where the bar indicates an averaging over pairs in a cell. If the definitions given before are substituted into Eq. (10), it can be seen that it is consistent with Eq. (9), the gas kinetic result.

A key task in performing the simulation is to efficiently select pairs of particles and evaluate whether a collision has taken place. In this section we consider nonreactive collisions. Hence, if a collision has occurred the velocities of the particles are changed according to the selected intermolecular force law. The determination of whether a collision has occurred is based on both the statistical or probabilistic element of the simulation and the total collision cross section. The number of pair selections of species (i, j) per cell in a time period Δt is $n_i Z_{ij} \Delta t$. Equation (10) shows that when we use a weighting scheme we are multiplying the collision frequency by W_j. Hence, if particle i is a trace species and particle j is a major species, then the trace species changes its velocity. Alternatively, if particle i is a major species and particle j is a trace species, it is unlikely that i will change its velocity. This is consistent with the concept of major and trace species because the major species properties are supposed to be independent of the presence of trace species.

In the work of Ivanov and Rogasinsky,[12] an efficient procedure was developed to simulate the collision procedure. This scheme, known as the majorant frequency scheme (MFS), redefines the collision frequency used in the simulation as

$$Z_{ij}^{\text{MFS}} = n_j [\sigma_T(v)v]_{\max} W_j \tag{11}$$

The collision frequency in a cell is calculated using the number of simulated molecules in the cell and the maximum value of the product of the total collision cross section and the relative collision velocity. The number of potential collision pairs is, therefore, maximized with respect to the product of the cross section and the relative velocity. Once a pair is selected, the probability that a collision occurs is evaluated by an acceptance–rejection test of the ratio of

$$P = \frac{\sigma_T(v)v}{[\sigma_T(v)v]_{\max}} \tag{12}$$

The number of collisions between pairs (i, j) is then

$$N_{ij}^{\text{coll,MFS}} = n_i Z_{ij}^{\text{MFS}} \Delta t P = n_i Z_{ij}^{\text{MFS}} \Delta t \left\{ \frac{\overline{\sigma_T(v)v}}{[\sigma_T(v)v]_{\max}} \right\} \tag{13}$$

which is consistent with Eq. (8).

To perform simulations more efficiently, let us suggest a modified form of the number of potential collision pairs:

$$N_{ij}^{\text{MFS}} = W_{\max} n_i n_j [\sigma_T(v)v]_{\max} \Delta t \tag{14}$$

where $W_{\max} = \max(W_i, W_j)$. Once a pair is selected, the probability that a collision occurs is evaluated by an acceptance–rejection test of P given in Eq. (12). If accepted, a second acceptance–rejection test is performed of the ratio of $P' = W_j / W_{\max}$ for i species and $P' = W_i / W_{\max}$ for j species. The total number of collisions is then $N_{ij}^{\text{MFS}} P P'$, and the collision frequency is $W_{\max} n_j [\sigma_T(v)v]_{\max} P P'$, which can be shown by similar substitutions of the original set of

definitions to reduce to the gas kinetic result. This procedure has been found to be particularly efficient for collisions between trace species.

C. Weighting Scheme for Chemical Reactions in a Gas

Because weights have been shown to be efficient in simulating elastic collisions, we consider their application to chemically reactive collisions. Let us consider the reaction

$$A + B \rightarrow C + D$$

where A, B, C, and D are species with weights W_A, W_B, W_C, and W_D, respectively. The rate equation for the change of concentration of species C is written in the usual gas kinetic form as

$$\frac{dn_c'}{dt} = k_r' n_A' n_B' \tag{15}$$

where k_r' is the rate coefficient

$$k_r' = \overline{\sigma_r'(v)v} \tag{16}$$

Here σ_r' is the reaction cross section, and in the simulation we use

$$\sigma_r = \sigma_r' F_{num} \tag{17}$$

As we discuss the simulation procedure for chemical reactions, we will find it useful to further define a reaction probability, $P_r' = P_r$, as

$$P_r \equiv \sigma_r / \sigma_T \tag{18}$$

Substitution of Eqs. (7), (17), and (18) into Eq. (15) gives the rate of formation of simulated particles C as

$$\frac{dn_c}{dt} = P_r \overline{\sigma_T(v)v} \frac{W_A W_B}{W_C} n_A n_B \tag{19}$$

When the simulations are performed, it is found useful to reexpress the reaction rate for simulated particles as

$$\frac{dn_c}{dt} = X_C W_{max} P_r \overline{\sigma_T(v)v} n_A n_B \tag{20}$$

where $W_{max} = \max(W_A, W_B)$ and X_C is the fraction of C simulated particles formed by the reaction and whose exact form can be obtained by equating Eqs. (19) and (20) as

$$X_C = \frac{W_A W_B}{W_{max} W_C}, \qquad \text{and, similarly,} \qquad X_D = \frac{W_A W_B}{W_{max} W_D} \tag{21}$$

The fractions of the particles of species A and B that will remain in the flow after the reaction are

$$X_A = 1 - W_B / W_{max}, \qquad X_B = 1 - W_A / W_{max} \tag{22}$$

Note that X_C and X_D may be greater than one if A and B are major species and C and D are trace species. In this case, Eq. (20) predicts a net increase in the number of C (and D) species.

Now we discuss the specific implementation of the MSF procedure to chemical reactions. First consider the number of pair selections N_{AB}^{MFS}, which, similar to Eq. (14), is defined as

$$N_{AB}^{MFS} = (W_{max\,2} / W_{min}) n_A n_B \sigma_T(v)_{v_{max}} \Delta t \tag{23}$$

where $W_{min} = \min(W_C, W_D)$ and $W_{max2} = \max[\min(W_A, W_B), \min(W_C, W_D)]$. For each selected A,B pair an acceptance–rejection test is performed for the probability of a collision, $\{\sigma_T(v)v / \sigma_T(v)v)_{max}\}$. If the pair is selected for a collision, we then evaluate whether a chemical reaction occurs. The criterion for a chemical reaction to occur is that the total collision energy be greater than the Arrhenius threshold energy and that the reaction probability P_r satisfies an acceptance–rejection test.

The rate of formation of species C is modeled in the MFS procedure as

$$\frac{dn_c^{MFS}}{dt} = \chi_c \frac{W_{max\,2}}{W_{min}} P_r n_A n_B \overline{\sigma_T(v)v} \tag{24}$$

where χ_C^{MFS} can be obtained by equating Eqs. (24) and (19) to give

$$\chi_C^{MFS} = \frac{W_A W_B}{W_C} \frac{W_{min}}{W_{max\,2}} \qquad \text{or} \qquad \chi_D^{MFS} = \frac{W_A W_B}{W_D} \frac{W_{min}}{W_{max\,2}} \tag{25}$$

If a chemical reaction occurs, the fraction of particles C and D added (or created) to the flow is χ_C^{MFS} and χ_D^{MFS}, respectively. The fraction of particles A and B removed from the flow is calculated as

$$\chi_A^{MFS} = 1 - \frac{W_B W_{min}}{W_{max\,2}}, \qquad \chi_B^{MFS} = 1 - \frac{W_A W_{min}}{W_{max\,2}} \tag{26}$$

If a chemical reaction does not occur, then the fractions of particles A and B whose postcollisional velocities change are $W_B W_{min} / W_{max\,2}$ and $W_A W_{min} / W_{max\,2}$, respectively.

It can be seen that the MFS procedure reduces to the gas kinetic result as follows. From Eq. (23), the rate of change of N_{AB}^{MFS} may be written as

$$\frac{dN_{AB}^{MFS}}{dt} = \frac{W_{max\,2}}{W_{min}} n_A n_B [\sigma_T(v)v]_{max} \tag{27}$$

and the rate of change of C may be related to the rate of change of N_{AB}^{MFS} as

$$\frac{dn_c}{dt} = \frac{dN_{AB}^{MFS}}{dt} \cdot \left\{ \frac{\overline{\sigma_T(v)v}}{[\sigma_T(v)v]_{max}} \right\} \cdot \{\chi_c P_r\} \tag{28}$$

where the first set of brackets represents the probability that the pair has been accepted and the second is the probability that a chemical reaction has occurred. Substitution of Eqs. (25) and (27) into (28) gives Eq. (19), which was shown to be equivalent to the gas kinetic result.

D. Weighting Scheme for Gas/Surface Chemical Reactions

Weights were also used to simulate gas/surface reactions for the following two types of processes:

$$A + B_S \rightarrow C \tag{29}$$

$$A + B_S \rightarrow A + B \tag{30}$$

where the subscript S represents a species absorbed on the surface. The first reaction represents the formation of a new chemical species C and the second represents an ejection process, also known as scrubbing. As discussed in the preceding section, the rate equations for species C in molecular and simulated particle form can be expressed as

$$\frac{dn_c'}{dt} = \sigma_f' n_A' n_{B_S}' \tag{31}$$

$$\frac{dn_c}{dt} = \sigma_f \frac{W_A W_B}{W_C} n_A n_{B_S} = \sigma_f X_C n_A n_{B_S} \tag{32}$$

where the reaction cross section σ_f' is related to the simulated cross section as before, $\sigma_f = \sigma_f' F_{num}$, and $X_C = W_A W_B / W_C$ is the fraction of particles of species C to be created after the reaction (and can be > 1). As before, the fractions of particles A and B that remain are

$$X_A = 1 - W_B / W_A, \qquad X_{B_S} = 1 - W_A / W_B \tag{33}$$

Similarly, for the scrubbing reaction, the fraction of desorbed particles of species B from the surface is

$$X_B = W_A W_B / W_B \tag{34}$$

These weighting schemes for gas and gas/surface interactions have been applied successfully for modeling chemical reactions in

trace species whose concentrations are many orders of magnitude smaller than those of major species. Note that the use of weighting factors is shown to be beneficial to obtain credible data with a low statistical scatter for reasonable computational times. The weighting schemes enumerated here enabled us to reduce the computational time by at least an order of magnitude as compared with previous efforts.[3]

E. Details on Modeling of Surface Reactions

In addition to adsorption and glow reactions, scrubbing reactions were also included in the DSMC algorithm. Calculation of the surface coverage was carried out in the following manner. During the simulation, the number fluxes were calculated for all gas species and for all surface elements. The calculation is repeated every N_c time steps, where N_c was chosen from 200 to 500, depending on the number of simulated molecules. A special smoothing procedure has been used to reduce the impact of statistical fluctuations. At time step N the number flux of ith species to be used in calculation of the surface coverage is

$$f_i = \frac{\varepsilon \sum_{s=1}^{N-N_C} f_{i,s}}{N - N_C} + \frac{(1-\varepsilon)\sum_{s=N-N_C+1}^{N} f_{i,s}}{N_C}$$

where $f_{i,s}$ is the number flux of ith species at time step s, and ε is a parameter determining the contribution of the first $N - N_c$ time steps ($\epsilon = 0.1$ was chosen here). Note that such a procedure reduces significantly the fluctuations of number fluxes and enables one to reduce simulation time. After the number fluxes are obtained, the surface coverage is calculated using the equation

$$S_{oi} f_i \left(1 - \frac{n_{i,s}}{n_T}\right) - k_b n_{i,s} - \sum_i f_i(\sigma_g n_{i,s} + \sigma_s n_{i,s}) = 0 \qquad (35)$$

where S_{oi} is the sticking coefficient of the ith species, $n_{i,s}$ is the number density of adsorbed molecules of species i, and σ_g and σ_s are the glow and scrubbing reaction cross sections, respectively ($\sigma_g = \sigma_{f3,f4}$). The surface coverage is the ratio of $n_{i,s}$ to the total number of surface sites n_T.

By the use of surface coverage and number fluxes, adsorption, glow, and scrubbing reaction probabilities are calculated for all surface elements (the detailed equations for all of the processes are given in earlier work[3]). The corresponding number flux of desorbed molecules is also calculated. Then, these probabilities are used over the next N_c time steps.

The glow reactions are modeled as a two-step process. First, NO_2^* molecules are created on the surface as a result of a gas-phase O and NO interaction with NO and O adsorbed on the surface. Then, NO_2^* molecules move out of the surface and radiate with the probability proportional to τ_l^{-1}, where τ_l is the NO_2^* lifetime. A radiation lifetime of 0.0003 s was used.

F. Analytic Tangent Slab Approximation

A tangent slab approximation[3] has been used in this work for comparison with DSMC solutions that model the radiative decay of NO_2^*. Note first that for the AE geometry the observations were made looking through the glow. The total intensity I in units of photon/cm^2 s can be expressed in terms of the spatial distribution of NO_2^* number density N as

$$I = \int_0^{2\pi}\int_0^{\infty} \frac{1}{4\pi}\frac{N(x)}{\tau_l}\,dx\,d\Omega = \frac{1}{2}\int_o^{\infty}\frac{N(x)}{\tau_l}\,dx \qquad (36)$$

where $x = 0$ corresponds to the position of the surface. Equation (36) represents the tangent slab approximation, implying that the integration over $d\Omega$ may be reduced to 2π. The steady-state distribution of $N(x)$ may be written as

$$\frac{\partial(Nv)}{\partial x} = -\frac{N}{\tau_l} \qquad \text{or} \qquad N(x) = C_0 \exp\left(-\frac{x}{\tau_l v}\right) \qquad (37)$$

Here, v is the gas velocity, and the variable of integration C_0 is the value of N at $x = 0$ and is equal to N_s'/v. Here, N_s' is the generation rate of NO_2^* on the surface. Substitution of Eq. (37) into Eq. (36) gives the tangent slab relation

$$I = \left(\sigma_{f3} n_{NO_s} f_O + \sigma_{f4} n_{O_s} f_{NO}\right)/2 \qquad (38)$$

where f_O and f_{NO} are the fluxes of O and NO to the surface, n_{NO_s} and n_{O_s} are the surface number density (molecules/m^2) of NO and O adsorbed on the surface, and σ_{f3} and σ_{f4} are the cross sections for Eqs. (3) and (4). Note that in the tangent slab approximation, the intensity is not a function of the radiative lifetime τ_l. Hence, if the tangent slab approximation can be shown to be close to the exact expression, Eq. (36), there is no requirement to know the lifetime of the excited state with high accuracy.

IV. Flow Conditions and Parameters of the Approach

The flow about AE at different flight altitudes has been studied. The flow is assumed to be two-dimensional, and the AE geometry is represented by a 2-m-diam cylinder. The freestream conditions are summarized in Table 3. The freestream conditions for the major species are from Jacchia,[13] and those for the trace species are from a sounding rocket experiment.[14] The speed of 7922 m/s was utilized for all altitudes. The surface temperature was 300 K.

Because the flow is symmetric, only half of the domain was considered, with the specular conditions at the symmetry plane. Diffuse reflection with the complete energy and momentum accommodation on the surface was assumed. The variable hard sphere model[2] was used for modeling molecular collisions, and the Borgnakke and Larsen model[15] with $Z_r = 5$ and $Z_v = 50$ was employed for energy exchange between the translational and internal modes. The number of simulated particles was about 100,000, and the number of cells was 20,000. The mean free path at 260 km is of the order of 1 km, and the cell size (of the background collisional grid) is approximately 1 m. The number of molecules per cubic mean free path (3×10^7 in the freestream) used in the computations satisfies standard DSMC requirements of the minimum cell size[2] and number of molecules.[16] The time step of 3×10^{-5} s was chosen so that simulated particles do not cross more than one cell per time step. Preliminary computations showed that the macroparameters and distributions do not change after 0.3 s. Until this time, the flow is unsteady and parameters are not sampled or averaged.

The most important gas-phase reaction that influences the radiation process was found to be

$$N_2 + O \rightarrow NO + N \qquad (39)$$

To study the sensitivity of the glow NO_2^* radiation to the cross section for this process, two different models were used. The first is the total collision energy (TCE) model,[2] and the second is the model developed by Bose and Candler[17] where the reaction cross sections were obtained basing on quasi-classical trajectory (QT model) calculations.

Two different sets of surface parameters were used as is indicated in Table 1. The two sets differ in the values of the heat of absorption for NO and the scrubbing cross section.

Table 3 Freestream conditions

H	$n \times 10^{16}$, m^{-3}	T, K	$O_2 \times 10^{-2}$	N_2	O	NO $\times 10^{-5}$	N $\times 10^{-3}$
140	9.354	625	6.18	0.65	0.29	8	0.05
150	5.307	733	5.46	0.62	0.33	9	0.2
160	3.350	822	4.86	0.58	0.37	11	1.04
170	2.260	878	4.33	0.55	0.40	14	2.1
180	1.619	947	3.89	0.51	0.44	18	3.08
190	1.207	980	3.49	0.49	0.47	15	4.6
200	0.906	1026	3.13	0.45	0.51	11	6.62

V. Results and Discussion

A. Effect of Gas-Phase Chemistry Model

Consider first the influence of the $N_2 + O \rightarrow NO + N$ reaction model on the flowfield and surface properties. The number density contours of nitric oxide at the altitude of 140 km are given in Fig. 1 for the TCE chemistry model (bottom half of Fig. 1) and QT model (upper half). Here and hereafter, surface set 2 has been used, except where specified otherwise. The computations show that the use of the more rigorous QT model results in a factor of two increase in the concentration of NO. The increasing of concentration, nevertheless, does not change the shape of the bow shock.

Because there are few collisions and, therefore, reactions, at high altitudes, chemical reactions between major species have little influence on changing the composition of the major species. This is illustrated in Fig. 2 where contours of the total number density are shown for the two chemistry models. Even though the number of reactions differs by a factor of more than two, the total number density profiles are almost identical. This is also true for the surface fluxes of all major species. The only freestream species affected by the choice of reaction model are NO and N.

The quantitative effect of the chemistry model on the NO surface number flux is illustrated in Fig. 3. The number flux profiles are presented along the surface, and the abscissa represents the distance

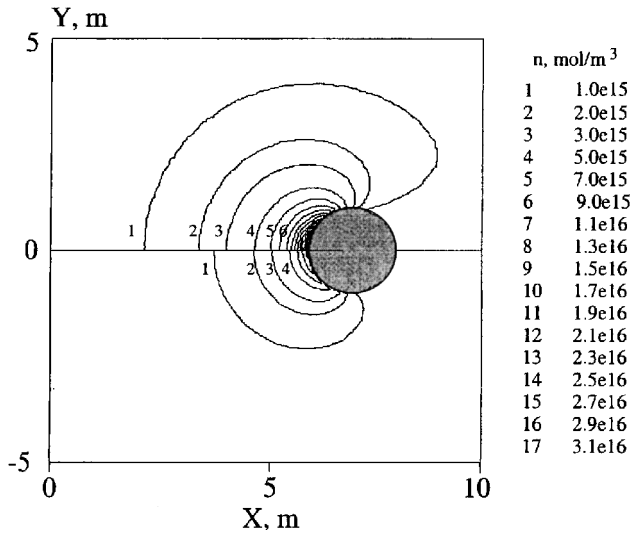

Fig. 1 NO number density fields for two chemistry models at 140 km; bottom and top halves are the TCE and QC models, respectively.

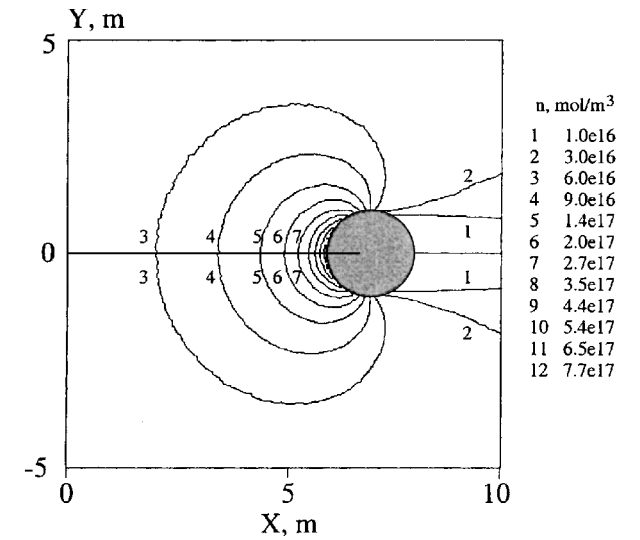

Fig. 2 Total number density for two chemistry models at 140 km; plots defined as in Fig. 1.

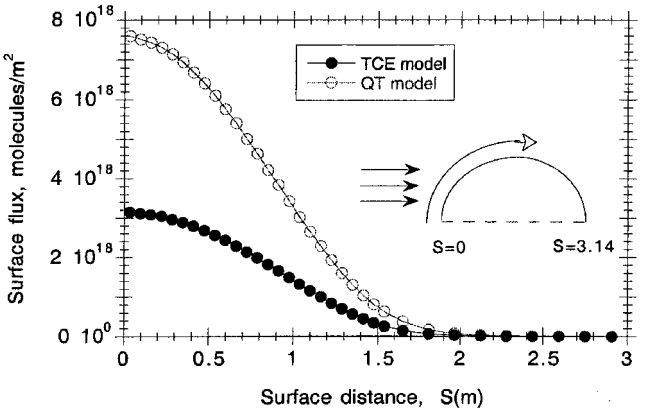

Fig. 3 NO surface number flux for two chemistry models at 140 km.

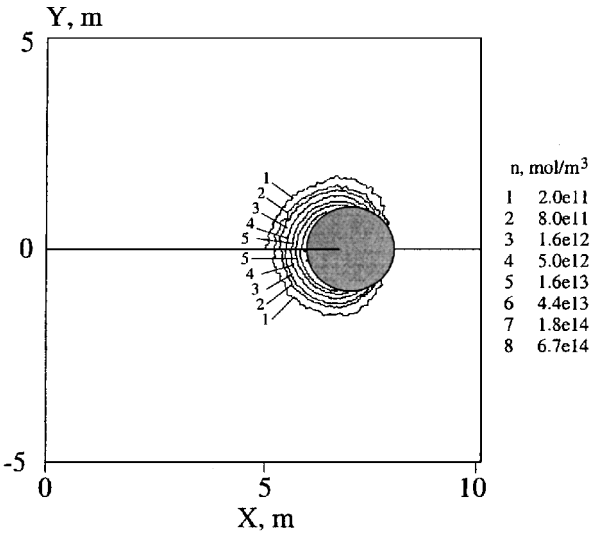

Fig. 4 NO_2^* number density for two chemistry models at 140 km; bottom and top halves are the TCE and QC models, respectively.

from the stagnation point (point 0) in meters along the body surface (surface length is 3.14 m). The number flux increases by a factor of 2.5 throughout the surface for the QT model, which is consistent with its larger reaction cross section for this model at the conditions under consideration.

The formation of radiating NO_2^* species on the surface is mostly determined by Eq. (3) rather than Eq. (4) because atomic oxygen has a low heat of adsorption compared to NO. The key parameters that influence the NO_2^* radiation are, therefore, the atomic oxygen flux on the surface and NO surface coverage. The atomic oxygen flux is not affected by the chemical reaction model. The NO surface coverage, however, depends on the NO surface flux and therefore, changes when the number of NO formation reactions [Eq. (39)] is changed. Because the number of reactions increases considerably for the QT model, the production of NO_2^* increases proportionally. This effect is shown in Fig. 4 where the NO_2^* number density is given. The density decreases drastically away from the body due to NO_2^* radiative decay.

The chemistry model effect on glow radiation produced by NO_2^* at altitudes of 150 km and higher is similar to that observed for 140 km. Comparison of the radiance values along the stagnation line is given in Fig. 5 for different altitudes from 140 to 200 km. The QT model predicts a higher level of radiation for all of the altitudes, with approximately the same factor of about 2.5 observed for the NO surface flux and NO_2^* number density.

The computations, therefore, show the importance of using an appropriate model for the reaction $N_2 + O \rightarrow NO + N$, the single mechanism responsible for gas-phase NO production. The choice of the reaction model becomes especially important for altitudes

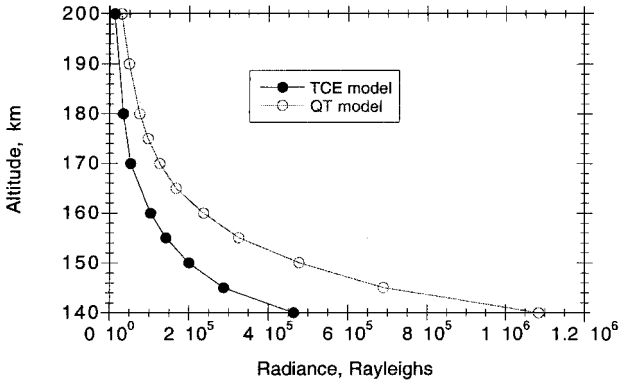

Fig. 5 Radiance in Rayleigh vs flight altitude for two chemistry models.

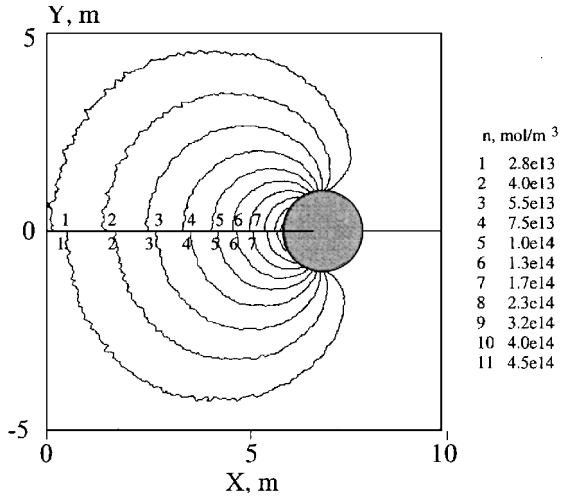

Fig. 6 NO number density fields for QT model with (top) and without (bottom) freestream NO at 200 km.

where the source of nitric oxide from chemical reactions in the shock layer dominates the nitric oxide of the freestream. That was observed for all altitudes under consideration, with the chemistry model influencing mainly the magnitude, but not the shape of the altitude dependence of the radiance. The significance of the freestream NO concentration is considered in the next section.

B. Importance of Freestream NO

As mentioned, the NO_2^* glow radiation principally originates from the interaction of gas-phase O bombarding adsorbed NO. Because atomic oxygen is a major species, it is not affected at high altitudes by chemical reactions or temporal variations of the freestream density. However, both of these processes may be of great importance for NO. Nitric oxide molecules adsorbed on the surface come from two sources, the freestream and the gas chemical reactions. The potential contributions of these two sources to the radiation is clarified hereafter.

To study the influence of freestream NO concentration on NO_2^* radiation, the computations were performed with and without freestream NO. Because the number of reactions (and, therefore, the chemistry contribution to the radiation process) decreases when altitude increases, an altitude of 200 km was chosen to study the maximum sensitivity to the freestream NO concentration. Again, the most important and the most influenced parameters are those connected with the NO concentration. Consider first the QT model. The NO number density fields for this model with and without freestream NO are given in Fig. 6. The obvious conclusion is that the inclusion of the freestream NO is visible but not a significant factor for the given conditions.

To provide a quantitative measure of difference between the two cases, a comparison of NO surface number fluxes using the QT model for these two computations is presented in Fig. 7. The results show that there is a fairly small, less than 10%, reduction in the NO surface flux when there is no NO in the freestream. The impact on NO surface coverage and radiation is proportional to the NO surface fluxes.

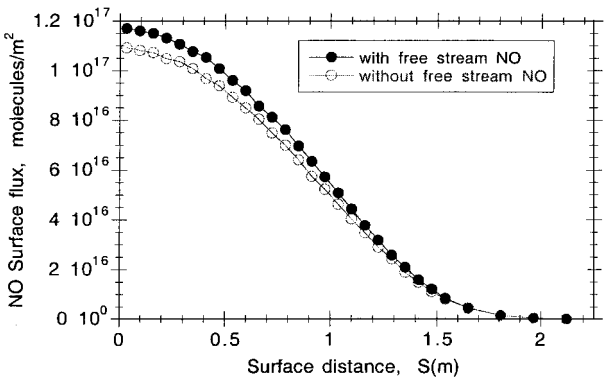

Fig. 7 NO surface number flux with and without NO in the freestream using the QT model at 200 km.

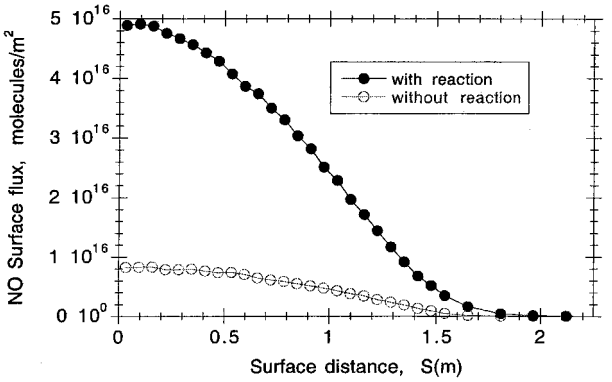

Fig. 8 NO surface number flux with and without the $N_2 + O \rightarrow NO + N$ reaction using the TCE model at 200 km.

A similar comparison aimed at the extraction of the role of freestream NO and NO created in chemical reactions was performed for the TCE model. In this case, two different cases were considered, with and without the reaction Eq. (39). Figure 8 shows that the freestream NO influence is larger than for the QT model. This is because the reaction cross section is smaller in the TCE model. However, the freestream NO concentration is still a much smaller source of NO than chemical reactions in the bow shock. This result is consistent with that obtained in earlier work[3] for the TCE model at 140 km. The improvements in the numerical accuracy presented here enable the comparison in the present work at 200 km, where the resolution of the events is more difficult than at 140 km.

With increasing density (lower altitudes) the relative influence of bow-shock chemical reactions as a source of NO increases in comparison to the contribution from the freestream. Therefore, for the range of altitudes considered (140–200 km), NO produced by chemical reactions remains the dominant source. Uncertainties in the ambient atmosphere NO measurements and databases is not likely to affect the glow radiance.

C. Comparison of the Full Flow Radiation Simulation with the Tangent Slab Approximation

An important issue in the glow analysis is the ability to predict radiation using readily available gas-phase surface fluxes of different species. One of the simple and efficient models for such an analysis is the model based on the tangent slab approximation, Eq. (38). This model is based on the one-dimensional treatment, and its applicability and accuracy for two- and three-dimensional flows depends approximately on the ratio of the shock radiating area to its standoff distance from the body.

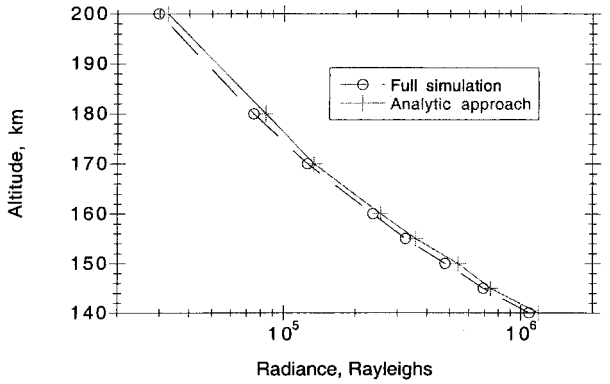

Fig. 9 Comparison of radiation (Rayleigh) obtained with the full simulation and the tangent slab analytical approach along the AE stagnation streamline.

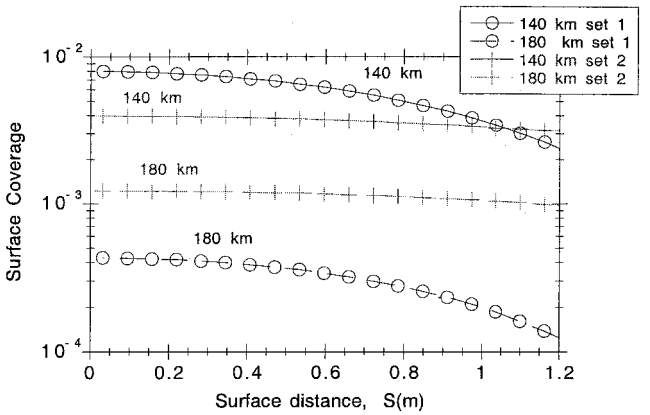

Fig. 10 NO surface coverage along the spacecraft surface.

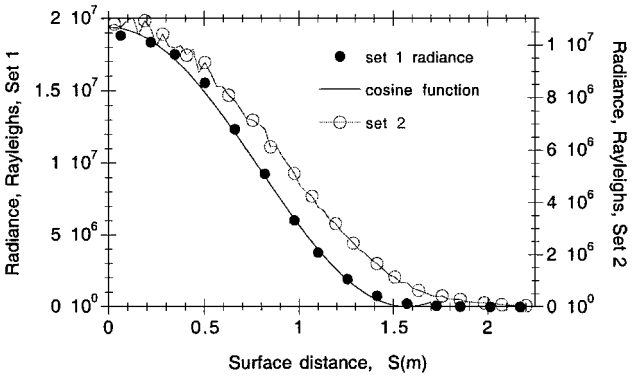

Fig. 11 Radiation along the surface for two surface sets; line represents a cosine dependence.

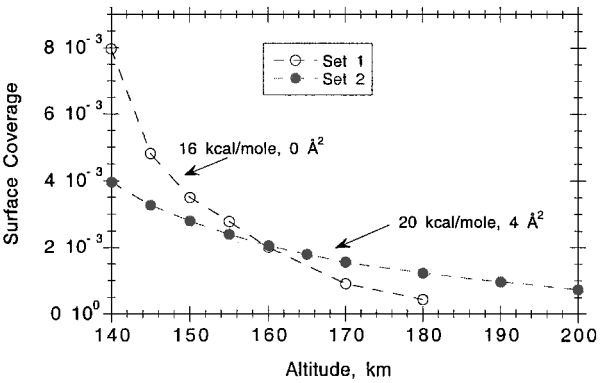

Fig. 12 NO surface coverage at the stagnation point for different surface sets.

To study the applicability of Eq. (38) in place of the full simulation, radiation calculated using the tangent slab approximation was compared with the full DSMC predictions at the stagnation point. The latter set of computations used the DSMC NO_2^* spatial distribution to numerically evaluate the first integral given in Eq. (36). Figure 9 shows such a comparison for the two calculations at different altitudes, using the QT chemistry model. The results for the NO_2^* radiance show a small, about 10%, overprediction of the analytic values. The difference is explained by the curvature of the AE geometry and inherent spatial spreading of gas flow, which makes the flow slightly different from a one-dimensional case.

To further confirm this result, additional computations were performed for a two-dimensional flat plate geometry at 140 km. The width of the plate was 1 m, which provided the flow structure close to one-dimensional near the stagnation line. Very good agreement between the full flow/radiation calculation and the tangent slab approximation was observed, with a radiance of 0.815×10^6 R for the full DSMC compared with 0.812×10^6 R for the tangent slab solution.

D. Effect of Scrubbing on Surface Coverage and Angular Dependence of Radiation

The computations indicated that the surface coverage changes qualitatively when the surface scrubbing mechanism, Eq. (5), is included. Figure 10 shows the surface coverage as a function of angle from the stagnation streamline for two altitudes, 140 and 180 km, and the two surface models. Similar angular dependence is observed for the surface coverage for the other altitudes. For both altitudes and surface models, the surface coverage can be seen to decrease monotonously from the stagnation point; however, the surface model set 2 shows a flatter angular dependence. The difference in angular dependence for the two surface models is due to the different contributions of freestream particles and particles that are reflected from the body. Because the surface coverage is proportional to the NO surface flux and inversely proportional to the major species surface flux (which cause the scrubbing), the NO surface coverage angular dependence is flatter than the no-scrubbing case. Note that we do not see this difference between the two models for adsorbed oxygen because its surface lifetime is too short for the impact of scrubbing to be important.

The radiance along the surface at 140 km is shown in Fig. 11 for the two surface models. For both cases the radiance has a maximum at the stagnation point and then gradually decreases along the surface. In Fig. 11, a comparison is also shown of the computed radiation profiles with a corresponding cosine law distribution, that is, $\cos^2(\alpha) \cdot \max(R)$. Here, $\max(R)$ is the computed maximum radiation (at the stagnation point), α is the angle between the OS line and the symmetry plane, and O is the center of the body. From Fig. 11 it can be seen that for the no-scrubbing case the computed radiance profile is very close to a cosine-squared dependence. At high altitudes the surface fluxes closely follow a cosine law dependence, and the NO_2^* formation is proportional to the product of NO and O surface fluxes. However, the dependence is more complicated when scrubbing is included, causing an observable difference between the computed radiance profile and the cosine law, as shown in Fig. 11.

Figure 12 presents the fractional surface coverage of NO as a function of altitude for both sets of surface parameters at the stagnation point. The altitude dependence of the two sets of results can be seen to be significantly different. For surface set 1 (no scrubbing) the decrease in the surface coverage of NO is mostly a consequence of the decreasing ambient gas density, which causes a reduction in the formation rate of NO in the gas-phase chemical reactions. The increase in the surface binding energy in surface set 2 should increase the fractional surface coverage. This effect is, however, offset by the removal of NO through scrubbing by the major species. The difference between the two sets in the fractional

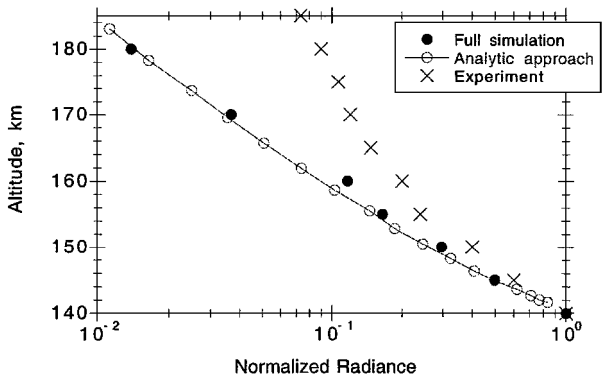

Fig. 13 Comparison of the altitude dependence for predicted (set 1) and measured radiances.

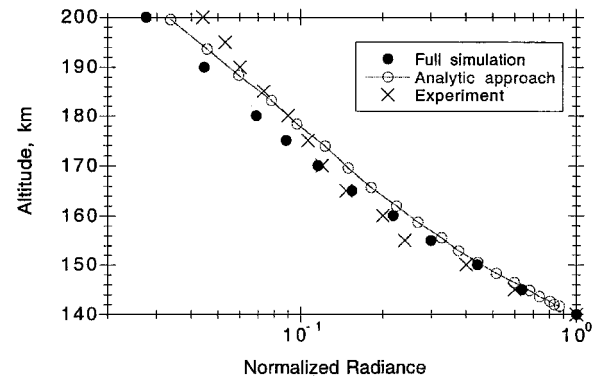

Fig. 14 Comparison of the altitude dependence for predicted (set 2) and measured radiances.

coverage of NO with altitude affects the altitude dependence of the radiation.

E. Comparison of Predicted Radiation with Experimental Data

Figures 13 and 14 compare the predicted radiation for different flight altitudes with the flight measurements of Yee and Abreu.[5] Analytic predictions presented here are a temporal solution of the surface reaction rates based on a specific AE orbit[3,5] using the DSMC surface fluxes obtained with the QT model. The normalized DSMC solutions for the TCE and QT models practically coincide. The analytic results are also close to those for the full DSMC; however, the slope is slightly different between 150 and 160 km. The experimental data predict a noticeable kink at about 155 km, which was not obtained in the model results. However, the slope of the normalized radiance for set 2 is much closer to the measurements than set 1. The dramatic slope change is due to the change in the surface scrubbing cross section. For the range of values considered here, the heat of absorption variation only changes the magnitude of the radiance vs altitude dependence and not the slope.

VI. Conclusions

The results of modeling visible glow radiation from NO_2 molecules about the AE in the transitional regime were presented. The range of altitudes from 140 to 200 km was studied. An improved, efficient, DSMC-based model was developed and used in the computations. The model enables one to simulate gas-phase reactions and sticking, glow, and scrubbing processes on the surface for major and trace species. The following conclusions can be drawn as a result of this study.

The use of the quasi-classical model[17] for the reaction $N_2 + O \rightarrow NO + N$ results in an increase of the radiance by a factor of 2.5 as compared to the TCE model, which is consistent with larger reaction cross sections given by the QT model. The altitude dependence of the predicted radiation is the same for either chemistry model.

The influence of the freestream NO concentration on the radiation is fairly small for all of the altitudes under consideration, and the main contribution to the radiation is the formation of NO in bow-shock gas-phase reactions. That suggests that the glow phenomena discussed here are not affected by the variations and uncertainties in the high-altitude atmosphere composition.

The comparison of computed radiances with experimental data shows that to predict the proper radiance vs altitude dependence, a nonradiative removal process of NO from the surface, that is, scrubbing, is required. As was found in our earlier work, the uncertainty in this fundamental gas/surface cross section dramatically affects the results.

Acknowledgments

This research was supported by the Army Research Office under Grant DAAG55-98-1-0236 and the Air Force Office of Scientific Research under Grant F49620-99-1-0143.

References

[1]Murad, E., "The Shuttle Glow Phenomenon," *Annual Review of Physical Chemistry*, Vol. 49, 1998, pp. 73–98.

[2]Bird, G. A., *Molecular Gas Dynamics and the Direct Simulation of Gas Flows*, Clarendon, Oxford, 1994.

[3]Dogra, V. K., Collins, R. J., and Levin, D. A., "Modeling of Spacecraft Rarefied Environments Using a Proposed Surface Model," *AIAA Journal*, Vol. 37, No. 4, 1999, pp. 443–452.

[4]Collins, R. J., Levin, D. A., and Dogra, V. K., "A Reexamination of the Atmospheric Explorer Data using the DSMC Technique," *Proceedings of the XX International Symposium on Gas Dynamics*, edited by R. Brun, R. Campargue, R. Gatignol, and J. C. Lengrand, Vol. 2, Cepadues-Editions, Toulouse, France, 1998, pp. 665–672.

[5]Yee, J. H., and Abreu, V. J., "Visible Glow Induced by Spacecraft–Environment Interaction," *Geophysical Research Letters*, Vol. 10, No. 2, 1983, pp. 126–129.

[6]Karipides, D. P., Boyd, I. D., and Caledonia, G. E., "Development of a Monte Carlo Overlay Method with Application to Spacecraft Glow," *Journal of Thermophysics and Heat Transfer*, Vol. 12, No. 1, 1998, pp. 30–37.

[7]Karipides, D. P., Boyd, I. D., and Caledonia, G. E., "Detailed Simulation of Surface Chemistry Leading to Spacecraft Glow," *Journal of Spacecraft and Rockets*, Vol. 36, No. 4, 1999, pp. 566–572.

[8]Swenson, G. R., Mende, S. B., and Clifton, K. S. "Ram Vehicle Glow Spectrum Implications of NO_2 Recombination Continuum," *Geophysical Research Letters*, Vol. 12, No. 2, 1985, pp. 97–100.

[9]Gasser, R. P. H., *An Introduction to Chemisorption and Catalysis by Metals*, Clarendon, Oxford, 1985.

[10]Gimelshein, S. F., Levin, D. A., and Collins, R. J., "Modeling of Infrared Radiation in a Space Transportation System Environment," AIAA Paper 2000-0731, Jan. 2000.

[11]Ivanov, M. S., Markelov, G. N., and Gimelshein, S. F., "Statistical Simulation of Reactive Rarefied Flows: Numerical Approach and Applications," AIAA Paper 98-2669, June 1998.

[12]Ivanov, M. S., and Rogasinsky, S. V., "Analysis of the Numerical Techniques of the Direct Simulation Monte Carlo Method in the Rarefied Gas Dynamics," *Soviet Journal of Numerical Analysis and Mathematical Modeling*, Vol. 3, No. 6, 1988, pp. 453–465.

[13]Jacchia, L. C., "Thermospheric Temperature, Density, and Composition: New Models," *Research in Space Science*, Smithsonian Astrophysical Observatory, Special Rept. 375, Cambridge, MA, March 1977.

[14]McCoy, R. P., "Thermospheric Nitrogen 1. NO, N(^4S), and O(^3P) Densities from Rocket Measurements of the NO δ and γ Bands and the O_2 Herzberg I Bands," *Journal of Geophysical Research*, Vol. 88, No. A4, 1983, pp. 3197–3205.

[15]Borgnakke, C., and Larsen, P. S., "Statistical Collision Model for Monte Carlo Simulation of Polyatomic Gas Mixture," *Journal of Computational Physics*, Vol. 18, No. 4, 1975, pp. 405–420.

[16]Gimelshein, S. F., Ivanov, M. S., and Rogasinsky, S. V., "Investigation of Shock Wave Structure by Majorant Cell and Free Cell Schemes of DSMC," *Proceedings of the XVII International Symposium on Rarefied Gas Dynamics*, edited by A. E. Beylich, VCH, Weinheim, Germany, 1991, pp. 718–726.

[17]Bose, D., and Candler, G. V., "Kinetics of the $N_2 + O \leftarrow NO + N$ Reaction Under Thermodynamic Nonequilibrium," *Journal of Thermophysics and Heat Transfer*, Vol. 10, No. 2, 1996, pp. 148–154.